Superhydrophilic surface modification of fabric via coating with cysteic acid mineral oxide

Wafaa Al-Shatty,[a,b] Donald A. Hill,[a] Sajad Kiani,[a] Andrius Stanulis,[a,c] Steve Winston,[d] Iain Powner,[e] Shirin Alexander,[a] and Andrew R. Barron*[a,f,g,h]

[a]*Energy Safety Research Institute (ESRI), Swansea University, Bay Campus, Swansea SA1 8EN, UK.*

[b]*Laboratory and Quality Control Department, Basrah Oil Company, Bab Al Zubair, Basrah 21240, Iraq*

[c]*Department of Electrochemical Materials Science, Center for Physical Sciences and Technology, Sauletekio Av. 3, Vilnius LT−10257, Lithuania*

[d]*MiDAS Green Innovation, Ltd., Swansea, SA1 8RD, UK.*

[e]*SALTS Healthcare, Ltd., Nechells, Birmingham B7 4AA, UK.*

[f]*Arizona Institutes for Resilience (AIR), University of Arizona, Tucson, Arizona 85721, USA.*

[g]*Department of Chemistry and Department of Materials Science and Nanoengineering, Rice University, Houston, Texas 77005, USA.*

[h]*Faculty of Engineering, Universiti Teknologi Brunei, Brunei Darussalam.*

HIGHLIGHTS

- Woven and non-woven fabrics are made superhydrophilic by the coating with cysteic acid functionalized metal oxide (CAMO) nanoparticles
- Untreated spunlace polypropylene (contact angle = 147.5°) shows the greatest change after CAMO treatment to a water absorption time of 15 ms.
- Aluminum oxide core provides superior performance over the homologous iron oxide nanoparticle cores.

* Corresponding authors at: Energy Safety Research Institute (ESRI), Swansea University, Bay Campus, Swansea SA1 8EN, UK

* E-mail: a.r.barron@swansea.ac.uk (Andrew R. Barron).

* ORCHID ID: Wafaa Al-Shatty: 0000-0002-3389-0199; Donald A. Hill; 0000-0002-3457-5895; Sajad Kiani: 0000-0003-1609-6855; Andrius Stanulis: 0000-0003-3827-2733 Shirin Alexander: 0000-0002-4404-0026; Andrew R. Barron: 0000-0002-2018-8288

ABSTRACT

Hypothesis: Cysteic acid functionalized mineral oxide nanoparticles can be used to impart superhydrophilic performance on a range of woven and non-woven fabrics.

Experiments: Woven and non-woven fabrics spray and dip coated alumina and iron oxide based cysteic acid functionalized mineral oxide nanoparticles, were characterized by SEM, EDX and the change in water contact angle was measured or where the increased hydrophilicity was sufficiently great that the time for the adsorption of the water droplet was measured.

Findings: Fabrics showed a remarkable increase in the hydrophilicity upon coating with cysteic acid functionalized mineral oxide nanoparticles, although alumina-based materials performed better than the iron oxide homologs. Untreated spunlace polypropylene (contact angle = 147.5°) shows the greatest change after CAMO treatment to a water absorption time of 15 ms.

Keywords: cysteic acid, nano metal oxide, functionalization, fabric, coating, super hydrophilic surface.

1. Introduction

The efficacy of breathable, yet viral trapping fabrics are of increasing importance, particularly in light of the recent COVID-19 pandemic [1]. The need to use and provide personal protection such as face covering as well as effective ventilation in buildings via heating, ventilation, and air conditioning (HVAC) filtration systems is a global challenge [2]. Typical PPE is hydrophobic since it is primarily designed as splash protection of bodily fluids, while HVAC filtration levels are defined by particle size rejection. Neither was originally designed for airborne viral pathogens in aerosol droplets which has been shown to be the major risk factor of COVID-19 [3-5]. The small size of viruses and even the aspirated droplets ordinarily require a filter/fabric with a small pore size; however, this also limits airflow which makes breathing more difficult in the case of masks and increases energy costs for HVAC. In both cases it would be desirable to have a porous (breathable) fabric that traps viruses by a different mechanism than physical size [6].

One approach in providing viral protection would be the incorporation of an additive that possesses anti-viral properties. For example, copper (Cu) and silver (Ag) are known to have anti-viral properties [7-9], while a recent report suggests that immobilization of enzymes also has anti-viral potential [10]. Unfortunately, in the case of copper and silver the anti-viral activity reported

is based upon submersion of the treated substrate in a viral containing solution, and while complete destruction of the virus occurs it requires an extended timeframe of minutes to hours. Where silver and copper containing fabrics have been tested for viral flow there is no enhanced viral rejection when compared to untreated fabric. We propose that in order to create sufficient residence time of an aspirated droplet on an active antiviral agent, it is necessary to collapse the aspirated droplet onto the surface and thus expose the virus to the antiviral agent. To collapse aspirated droplets a hydrophilic surface or better still a superhydrophilic surface is required.

There have been a wide range of approaches to the creation of superhydrophilic fabrics, including depositing ultrathin silica layers [11], nanodiamond coatings [12], growing zinc oxide nanorods [13], attaching nanoparticles to pretreated fabric [14,15], as well as new polymer compositions [16]. We have previously reported that the surface energy of alumina-based materials can be altered using carboxylic acids with appropriate functional groups [17]. The application of a carboxylate functionality is dictated by relationship between the O···O distance in a carboxylic acid and the Al···Al distance in alumina materials [18,19], the resulting topotactic reaction ensures a covalent functionality. Thus, the surface of metal oxides can be tailored from superhydrophobic [20] to superhydrophilic [21] depending on the choice of the carboxylic acid: superhydrophilicity was best achieved with cysteic acid [22].

Additionally, we have shown that a similar surface modification can occur on micron- and nano-sized particles [23-25], which can be immobilized onto fibers and fabrics by dip coating and partial thermal annealing (ca. 100 °C) [21,26]. Previous results with Nomex fabric have demonstrated the coating ability, but the high "weight" (200 g/m^2) has a low airflow limiting its use outside specialist applications [27]. There is a need, therefore, to apply the concept of creating superhydrophilic functionalization to a wider range fabrics. In particular, non-woven and specifically spunlace polypropylene that are commonly used in filters. Herein report an investigation of dip and spray coating of cysteic acid functionalized metal oxide (CAMO) nanoparticles onto a range of non-woven fabrics and determined the conditions for optimization of the hydrophilic properties.

2. Experimental

2.1. Materials

Cysteic acid monohydrate ($C_3H_9NO_6S$) was obtained from Shaanxi Greenbo Biochem Co., Limited. Preformed alumina (13 nm) nanoparticles, Iron(II) chloride tetrahydrate ($FeCl_2.4H_2O$, 99%) and sodium hydroxide (NaOH, ≥ 97%) were purchased from Sigma-Aldrich and used as received. Pural SB pseudoboehmite was provided by Sasol Germany. Deionized water (resistivity = 18.2 MΩ cm, Millipore) was used to conduct the experiments.

2.2. *Alumina CAMO preparation*

Cysteic acid functionalized alumina particles were prepared by a modification of two previously reported methods [23,25]. In the first method, preformed alumina nanoparticles (13 nm, 130 g, 1.3 mol) were dispersed in 3.0 L of deionized water using mechanical stirring. An excess of cysteic acid (357 g, 2.1 mol) was then added and the mixture heated to reflux for 16 hours. Once the reaction time had elapsed, the mixture was allowed to cool in air until it reached room temperature. The solid from the mixture was recovered through centrifuging the suspension at 3800 rpm for one hour and then discarding the supernatant. Following this, the solid was re-suspended in deionized water and then sonicated for ten minutes in order to remove physisorbed cysteic acid from the particles. The solid was then recovered through centrifuging at 3800 rpm for one hour and discarding the supernatant. The particles were dried at 90 °C for 16 hours. The dry mass of the recovered solid was ca. 113 g. The products from this reaction are given the acronym Al_{NP}-CAMO. In the second method, boehmite powder (10.0 g, 0.167 mol) was dispersed in 100 mL of deionized water. 160 mL of 1.0 M cysteic acid solution (31.3 g, 0.167 mol) was added to the boehmite suspension. This resulted in formation of a viscous slurry. Therefore, 50 mL of deionized water were added to that mixture. The mixture was refluxed at 90 °C for 17 hours. The reaction flask was allowed to cool down to room temperature and then centrifuged for 25 min at 3800 rpm. The precipitate was washed with deionized water and then centrifuged. This was repeated twice. The precipitate was oven dried at 85 °C for 15 hours. The final product mass was 9.5 g. The products from this reaction are given the acronym Al_B-CAMO. A summary of alternative synthetic conditions is given in Table 1.

Table 1

Summary of a reaction conditions for the synthesis of Al-CAMO from either preformed alumina nanoparticles or boehmite.

Mineral	Mass (g)	Total volume H_2O (mL)	Cysteic acid (g)	Addition process	Time (h)	Yield (g)	Yield based upon mineral mass (%)
Alumina NP	130	3000	357	Add solid acid to mineral suspension	16	113	87
Alumina NP	10	450	28	Add acid solution to mineral suspension	21	12.2	122
Alumina NP	130	3000	357	Add acid solution to mineral suspension	19	140	108
Alumina NP	95.8	3000	264	Add acid solution to mineral suspension	22	101	105
Boehmite	10	2600	31.26	Add acid solution to mineral suspension	17	9.5	95
Boehmite	10	250	18.75	Add solid mineral to acid solution	21	9.4	94
Boehmite	100	2500	187.5	Add solid mineral to acid solution	21	108	108
Boehmite	10	250	6.25	Add solid mineral to acid solution	21	9.4	94

2.2. *Iron oxide CAMO preparation*

Cysteic acid functionalized iron oxide particles (Fe-CAMO) were prepared by a modification of a previously reported method [28,29]. A $FeCl_2.4H_2O$ solution (100 mL, 1.0 M) was magnetically stirred for 15 minutes, after which an aqueous NaOH solution (100 mL, 1.67 M) was added dropwise over a period of 1.5 hours, under vigorous stirring. Upon addition of the NaOH solution the color of the solution was observed to change from orange to brown, and then finally to black towards then end of the addition. Cysteic acid solution (80 mL, 1.0 M) was then added and the suspension heated to 90 °C for 16 hours under magnetic stirring. Once the reaction time had elapsed, the mixture was allowed to cool to room temperature. A black solid was then recovered from the mixture through centrifuging the suspension at 3800 rpm for one hour and discarding the supernatant. The solid was dried at 90 °C for four hours. The dry mass of the solid was approximately 7 g. A summary of alternative synthetic conditions is given in Table 2.

Unfunctionalized iron oxide particles (FeO_x-NP) were prepared by a modification of the above method. An aqueous $FeCl_2.4H_2O$ solution (100 mL, 1.0 M) was stirred for ca. 15 min, after which an aqueous NaOH solution (100 mL, 1.67 M) was added dropwise over ca. 2 h, with

continued stirring. During the addition of the NaOH solution the color of the suspension was observed to change from light green to brown, and then finally to black at the end of the addition. The solid from the suspension was recovered through centrifuging the mixture at 5000 rpm for 1 h and the supernatant discarded. The solid was then re-suspended in deionized water and sonicated for 10 min to remove adsorbed ions from the particles. Following this, the solid was recovered through centrifuging the mixture at 5000 rpm for 1 h and discarding the supernatant. This process of sonication in deionized water and recovery of the solid using centrifugation was repeated one further time using the same conditions. The material was then dried in an oven at 90 °C for 16 hours to afford a black solid.

Table 2

Summary of a reaction conditions for the synthesis of Fe-CAMO.

Volume (mL) of $FeCl_2$ solution (1 M)	Volume (mL) NaOH solution (1.67 M)	Reaction time (min.)	Volume (mL) of cysteic acid solution (1 M)	Reaction time (h)	Yield (g)	Yield based upon $FeCl_2$ mass (%)
100	100	90	80	16	7.0	55
100	100	210	80	16	5.2	41
100	100	120	3.8 g[a]	16	5.9	47
100	100	120	None	n/a	7.5[b]	58
100	100	210	80	21	4.3	34
100	100	220	80	21	3.2	25
100	100	220	80	21	4.1	32
980	980	150	800	16	26.6	21
1500	1500	270	1200	16	44.5	23
1500	1500	280	1200	16	31.3	16
1500	1500	270	1200	16	32.3	17
3000	3000	540	2400	20	47.6	13
3000	3000	240	2400	21	50.6	13
3000	3000	240	2400	16	63.2	17

[a] Added as a solid. [b] Unfunctionalized FeO_x NP.

2.3.*Characterization methods*

Fourier transform infrared attenuated total reflection (FTIR-ATR) analysis of csyteic acid functionalized mineral particles was made using Thermo Scientific Nicolet iS10 FT-IR Spectrometer in the 600-1800 cm^{-1} region, with 32 scans. Thermogravimetric analysis (TGA) was carried out using ca. 20 mg samples in an alumina pan with a TA Instruments SDT Q600 at a heating rate of 20 °C.min^{-1} from room temperature to 800 °C in air. Scanning electron microscopy (SEM) images equipped with energy dispersive X-ray analysis (EDX) were taken using a Hitachi

TM3000 tabletop microscope (Hitachi, Japan). Dynamic light scattering (DLS) analysis was used to measure the particle size distribution in deionized water using Zetasizer Nano ZS (Malvern).

2.4. *Fabrics selected for this study*

Six different types of fabrics were selected as substrates to be used during this investigation. These fabrics differed in both their density and chemical composition (Table 3). All fabrics were used as received and coated without carrying out any further treatment.

Table 3

Characterization of the as received fabrics. EDX analysis was performed using the SEM mentioned in section 2.3.

Fabric	Fabric weight (g/m^2)	Elemental Composition (EDX)	
		O / %	C / %
Woven polyethylene	131	66.09	33.91
Spunlace polypropylene	30	1.73	98.27
Spunlace polypropylene	55	36.50	63.50
Woven polyester Poplin	62	35.60	64.40
Woven polyester Montana	60	36.25	63.75
Woven polyester/spandex	120	30.69	69.31

2.5. *Dip coating*

In a typical experiment, a piece of the chosen fabric (3×3 cm^2) was dip coated in an aqueous suspension of appropriate cysteic acid functionalized mineral oxide nanoparticles for approximately 5 s. The fabric was then dried through heating in a drying oven under ambient atmosphere, to 100 °C for 2 hours. A summary of the various dip coating experiments, including the identity of the mineral oxide and the fabric as well as the solution concentration is provided in Table 4.

Table 4

Summary of a dip coat conditions for the synthesis of Al-CAMO coated fabrics.

Fabric	Fabric weight (g/m^2)	Al-CAMO	Solution conc. (wt.%)	Drying time (min.)
Woven polyethylene	131	Al_{NP}-CAMO	20	120
Spunlace polypropylene	30	Al_{NP}-CAMO	20	120
Spunlace polypropylene	55	Al_{NP}-CAMO	20	120
Woven polyester Poplin	62	Al_{NP}-CAMO	20	120
Woven polyester Montana	60	Al_{NP}-CAMO	20	120
Woven polyester/spandex	120	Al_{NP}-CAMO	20	120
Spunlace polypropylene	55	Al_{NP}-CAMO	1	20
Spunlace polypropylene	55	Al_{NP}-CAMO	2	20
Spunlace polypropylene	55	Al_{NP}-CAMO	5	20
Spunlace polypropylene	55	Al_{B}-CAMO	1	20
Spunlace polypropylene	55	Al_{B}-CAMO	2	20
Spunlace polypropylene	55	Al_{B}-CAMO	5	20

2.6. *Spray coating*

Two approaches were taken in the spray coating experiments. First, a piece of the chosen fabric (3×3 cm^2) was spray coated with an aqueous suspension of appropriate cysteic acid functionalized mineral oxide nanoparticles (M-CAMO) for approximately 1 s. This was carried out using a hydrocarbon airbrush propellant (Spraycraft SP10, 500 mL) and a spray gun nozzle (0.6 mm). As required subsequent layers were then sprayed onto the fabric for similar amounts of time. The fabric was then dried through heating in an oven in air to 100 °C for 20 minutes. In the second method a measured volume of a 1 wt.% solution was sprayed for 20 s. The fabric was then dried through heating in an oven in air to 100 °C for 20 minutes. In order to provide a comparison of the effect of the cysteic acid, samples of iron oxide nanoparticles (without cysteic acid) were sprayed under identical conditions. A summary of the various spray coating experiments, including the identity of the mineral oxide and the fabric as well as the solution concentration is provided in Table 5.

Table 5

Summary of a spray coat conditions for the synthesis of M-CAMO (M = Al, Fe).

Fabric	Fabric weight (g/m^2)	Nanoparticles	Solution conc. (wt.%)	Number of 1 s coat steps[b]	Volume (mL)[c]
Spunlace polypropylene	55	Al_{NP}-CAMO	1	3	n/a
Spunlace polypropylene	55	Al_{NP}-CAMO	2	3	n/a
Spunlace polypropylene	55	Al_{NP}-CAMO	5	3	n/a
Spunlace polypropylene	55	Al_{NP}-CAMO	1	3	n/a
Spunlace polypropylene	55	Al_{NP}-CAMO	5	1	n/a
Spunlace polypropylene	55	Al_{NP}-CAMO	1	n/a	5
Spunlace polypropylene	55	Al_{NP}-CAMO	1	n/a	10
Spunlace polypropylene	55	Al_{NP}-CAMO	1	n/a	15
Woven polyester/spandex	120	Al_{NP}-CAMO	1	1	n/a
Woven polyester Poplin	62	Al_{NP}-CAMO	1	3	n/a
Woven polyester Montana	60	Al_{NP}-CAMO	1	3	n/a
Spunlace polypropylene	55	Al_B-CAMO	1	3	n/a
Woven polyester Poplin	62	Al_B-CAMO	5	3	n/a
Woven polyester Montana	60	Al_B-CAMO	5	3	n/a
Spunlace polypropylene	55	Fe-CAMO	1	3	n/a
Spunlace polypropylene	55	Fe-CAMO	2	3	n/a
Spunlace polypropylene	55	Fe-CAMO	5	3	n/a
Spunlace polypropylene	55	FeO_x [a]	1	3	n/a
Spunlace polypropylene	55	FeO_x [a]	2	3	n/a
Spunlace polypropylene	55	FeO_x [a]	5	3	n/a
Woven polyester/spandex	120	Fe-CAMO	5	1	n/a
Woven polyester Poplin	62	Fe-CAMO	5	1	n/a
Woven polyester Poplin	62	Fe-CAMO	5	3	n/a
Woven polyester Montana	60	Fe-CAMO	5	1	n/a
Woven polyester Montana	60	Fe-CAMO	5	3	n/a

[a] Product from the reaction of $FeCl_2$ with NaOH without the addition of cysteic acid.

[b] The abbreviation "n/a" is used for samples that were not sprayed with the suspension sequentially in steps. Instead, the entire suspension volume is sprayed onto the fabric in one step.

[c] The abbreviation "n/a" is used for samples where the volume of the spray coating suspension was not measured, instead samples were sprayed in stages according to column five of the table and dried at 100 °C after each application of the coating.

2.7. *Contact angle measurements*

Static contact angle values were measured for solid-liquid interface using DSA25 Expert Drop Shape Analyzer and analyzed using ADVANCE software (KRÜSS GmbH) equipped with the automated camera at 25 °C and 35% humidity. The sessile drop method was performed for the purpose of measuring contact angle values according to the Young−Laplace equation, this was completed using a contour-fitting algorithm. Each of the contact angle measurements, and water adsorption measurements were repeated three times to minimize standard errors.

3. Results and discussions

3.1. Synthesis and characterization of Al-CAMO

As noted above, we have investigated two routes to the formation of cysteic acid functionalized alumina nanoparticles: (a) the surface functionalization of preformed 13 nm alumina nanoparticles [20] and (b) the reaction of pseudo boehmite in which the larger particles are reduced in size by the reaction [25]. During the reaction, cysteic acid is chemically absorbed onto aluminium oxide NPs and pseudo boehmite through covalent binding with surface sites [20]. Large scale synthesis of metal oxide NPs is often defined as multi gram [30-32]; however, both of these reactions have been performed previously at this scale and, we are interested in the possibility of scaling-up the reactions to >100 g.

For purposes of comparison, the percentage yield is defined as Eq. 1, where m_{Al} is the mass of the mineral source (NPs or boehmite) and m_{CAMO} is the mass of Al-CAMO isolated.

$$\text{Yield} = \frac{m_{CAMO}}{m_{Al}} \times 100 \qquad (1)$$

As may be seen from Table 1 the formation of Al_{NP}-CAMO by the addition of an aqueous solution of cystic acid to an aqueous suspension of preformed NPs shows a small decrease in yield (ca. 8%) upon a 10× increase in scale; however, further increases appear to not affect the yield, suggesting that larger scale reactions are possible without significantly lowering the isolated yield. Adding the cysteic acid as a solid to an aqueous suspension of preformed NPs lowers the yield, while the reaction appears to be independent of the relative concentration of either cysteic acid or NPs. This latter observation suggest that in large scale synthesis the ratio of reagents can be dictated by economic factors and the ease of purification of the product from any unreacted reagents.

In contrast to Al_{NP}-CAMO, the formation of Al_B-CAMO by the addition of an aqueous solution of cysteic acid to an aqueous suspension of pseudo boehmite shows a slight increase in isolated yield, (ca. 14%) upon a 10× increase in scale, again suggesting that the reaction is suitable for >100 g scale batches (see Table 1). Also, unlike the preformed NPs there is no effect of adding the cysteic acid as an aqueous solution to the aqueous suspension of pseudo boehmite or adding the latter as a solid to the aqueous solution of the former, allowing for a simpler reaction at scale. As with the preformed NP synthesis, the yield is independent of the cysteic acid:mineral ratio. In

fact, the yield is constant over a reagent ratio of 0.63:1 to 3.13:1 suggesting that the reaction can be performed irrespective of the reagent ratio.

The TGA characterization of samples prepared by the two methods show a marked difference in the extent of functionalization. As is seen in Fig. 1 the TGA for Al_{NP}-CAMO shows a 11.4% weight loss as compared to 34% for Al_{B}-CAMO. The lower weight loss is consistent with a low level of cysteic acid functionalization. The relative level of functionalization is consistent with the aggregate size (measured by DLS) which shows an average size of 65 nm and 50 nm for Al_{NP}-CAMO and Al_{B}-CAMO, respectively (Fig. 2). It is known that smaller aggregate size comes from more functional groups [33].

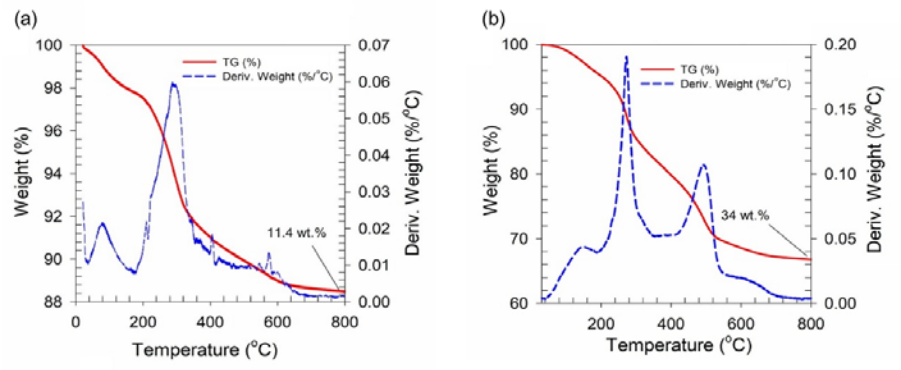

Fig. 1. Representative thermogravimetric analysis (TGA, red line) and associated derivative weight (blue dashed line) plots for (a) Al_{NP}-CAMO and (b) Al_{B}-CAMO prepared using 10 g of the appropriate mineral, heated under air at 20 °C/min.

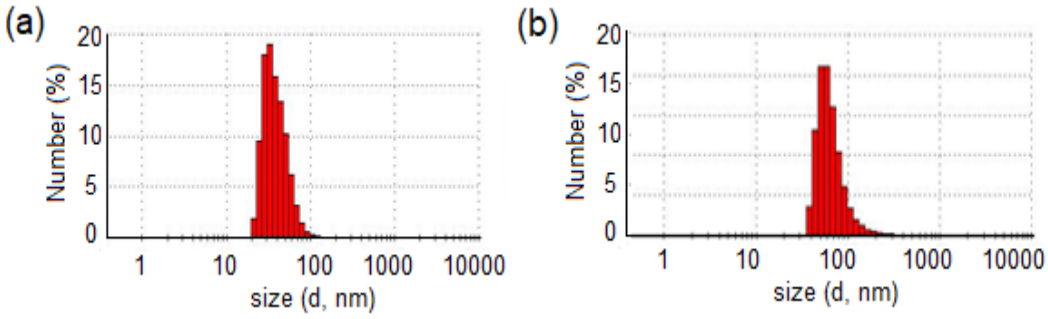

Fig. 2. Plots of particle size distribution for (a) Al_{NP}-CAMO and (b) Al_{B}-CAMO prepared using 10 g of the appropriate mineral.

In order to determine the inherent hydrophilic nature of Al_{NP}-CAMO, a microscope glass slide substrate (25×75 mm) was spray coated with 5 wt.% aqueous suspension of Al_{NP}-CAMO. The slide was then dried at 100 °C for 2 hours. The water contact angle of the coated glass substrate was ~7°. This is consistent with the value of 5° previously reported for Al_{B}-CAMO [21].

3.2. Synthesis and characterization of Fe-CAMO

Although carboxylic acids are known to react with Goethite (the iron analogue of boehmite) [34], we and others have shown that large scale synthesis of carboxylic acid functionalized iron oxide nanoparticles are best made from the formation of lepidocrocite from $FeCl_2$ [28,35] by the reaction with NaOH followed by reaction with cysteic acid (Scheme 1). Similarly to the synthesis of aluminum oxide functionalised by cysteic acid (Al-CAMO), the cysteic acid becomes chemically absorbed onto FeOOH (Fe-CAMO) during the reaction [29]. In the present study a 1 M solution of $FeCl_2$ was used in all the reactions, however, the scale is varied between 100 mL and 3000 mL of the solution. Other variables include the time after NaOH addition and prior to cysteic acid addition from 1.5 to 4.5 hours.

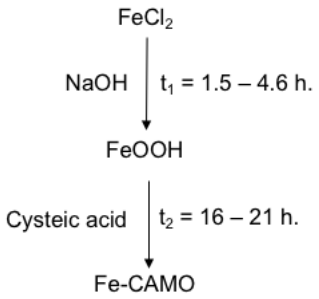

Scheme 1. Reaction steps for the formation of Fe-CAMO from $FeCl_2$.

As may be seen from Fig. 3a as the scale of the reaction is increased then the mass of Fe-CAMO isolated increases in a near linear manner; however, the percentage yield as derived from Eq. 2 decreases with increased scale (Fig. 3b). This suggest that a limited yield of ca. 13% in large scale production may be problematical unless the unreacted iron oxide can be recycled.

$$\text{Yield} = \frac{\text{mass}_{\text{Fe-CAMO}}}{\text{mass}_{FeCl_2}} \times 100 \qquad (2)$$

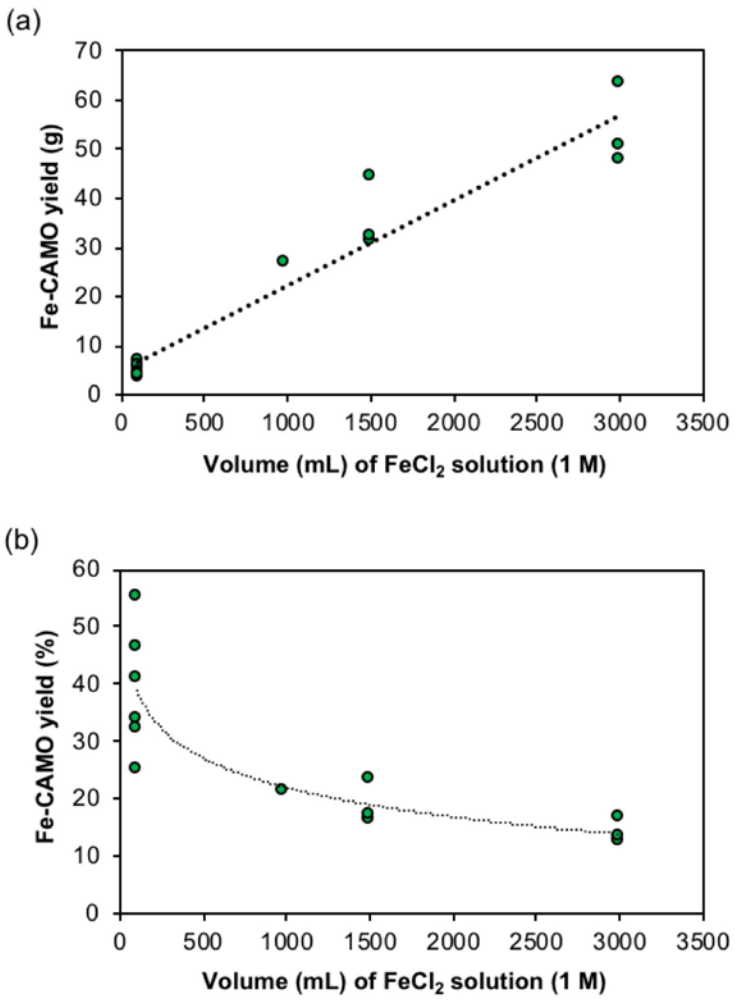

Fig. 3. Plots of Fe-CAMO yield in (a) mass ($R^2 = 0.92$) and (b) as a percentage as a function of the volume of a 1 M solution of $FeCl_2$.

Interestingly, as shown in Fig. 4, the yield decreases with increased time between the addition of the NaOH to the $FeCl_2$ and the addition of the cysteic acid, i.e., t_1 in Scheme 1. There is also a decrease in yield (albeit on a limited sample size) with increased reaction time after addition of cysteic acid, i.e., t_2 in Scheme 1.

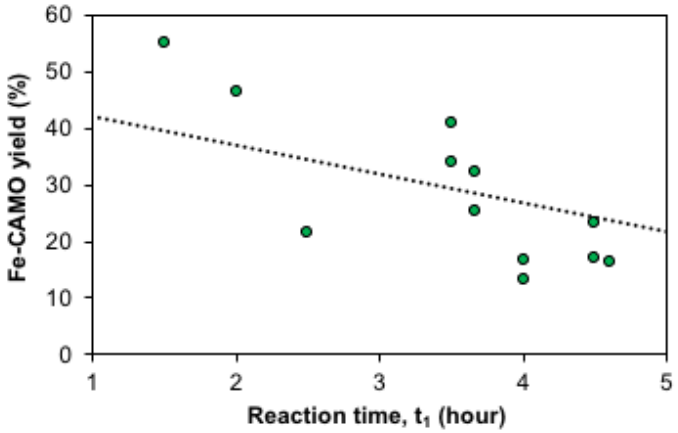

Fig. 3. Plot of Fe-CAMO yield as a percentage as a function of the time between the addition of aqueous NaOH to the $FeCl_2$ solution and the addition of the cystic acid solution.

The TGA data (Fig. 5) indicates a functionalization ratio for Fe-CAMO is similar to that of Al_{NP}-CAMO (c.f., Fig. 2), while the particle size distribution of Fe-CAMO becomes bi-modal upon longer time (t_1), see Fig. 6.

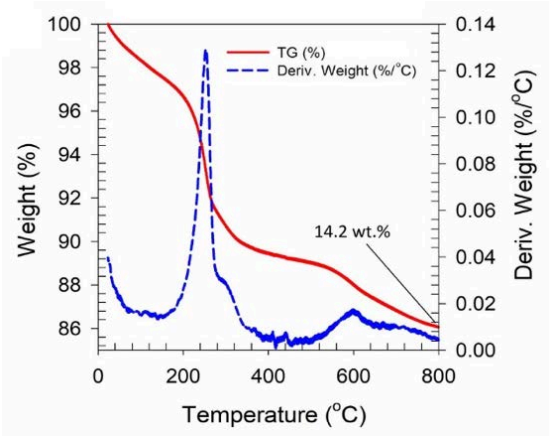

Fig. 5. Representative thermogravimetric/differential thermal analysis (TG/DTA) plots for Fe-CAMO nanoparticles heated under air at 20 °C/min.

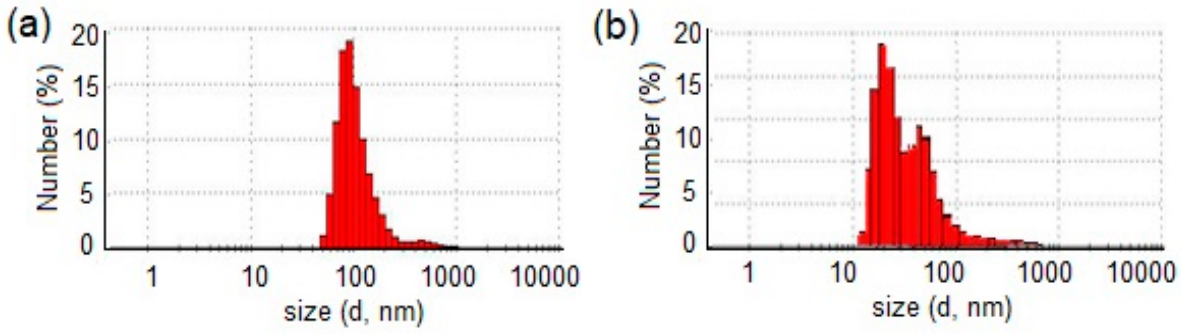

Fig. 6. Plots of the particle size distribution of Fe-CAMO as prepared using 100 mL of a 1M $FeCl_2$ solution, 100 mL of a 1.67M NaOH solution reacted for 3.5 hours before addition of 80 mL of 1M cysteic acid solution and reacting for (a) 16 h and (b) 21 h.

In order to determine the inherent hydrophilic nature of Fe-CAMO, a microscope glass slide substrate (25×75 mm) was spray coated with 5 wt.% aqueous suspension of Fe-CAMO. The slide was then dried at 100 °C for 2 hours. The water contact angle of the coated glass substrate was only ~115°. This is consistent with our prior work for superhydrophobic analogues, where the aluminum version shows a greater effect than the iron homologue [29].

3.3. Characterization of base fabrics

The uncoated fabrics were characterized by SEM and associated EDX analysis (see Supplementary Material and Table 3) to confirm their composition and hydrophilicity/hydrophobicity. In order to determine the baseline hydrophilicity/hydrophobicity of the fabrics the water contact angle was measured (e.g., Fig. 7). However, in some samples (the two polyester fabrics) the contact angle could not be measured since the water absorbed into the fabric (Fig. 8). Thus, the time taken for a water droplet placed on the surface to lose its structure and be absorbed by the fabric was determined in place of contact angle. The results are summarized in Table 6.

Table 6 Summary of the wettability of the as received fabrics.

Fabric	Fabric weight (g/m^2)	Water contact angle (°)[a]	Water absorption time (ms) [b]
Woven polyethylene	131	141	n/a
Spunlace polypropylene	30	147.5	n/a
Spunlace polypropylene	55	147.5	n/a
Woven polyester Poplin	62	n/a	10000
Woven polyester Montana	60	n/a	180
Woven polyester/spandex	120	144 – 147	n/a

[a] The abbreviation "n/a" is used to show that water droplets did not remain on the top of the fabrics and as a result the contact angles could not be measured. Instead, the droplets were absorbed into the fabric in the times stated in column four.

[b] The abbreviation n/a" is used to show that water droplets were not absorbed into the fabrics. Instead, they remained on the surface and showed the contact angles listed in column three.

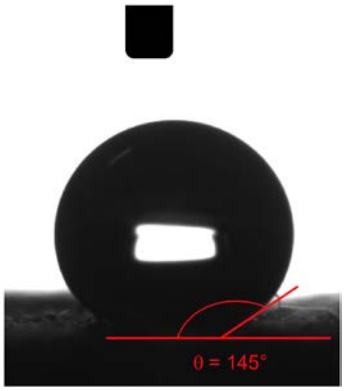

Fig. 7. Representative photograph of a 4.0 μL water droplet on the as received 120 g/m^2 woven polyester/spandex blend fabric, where the width of the needle (at the top of the image) is approximately 0.514 mm.

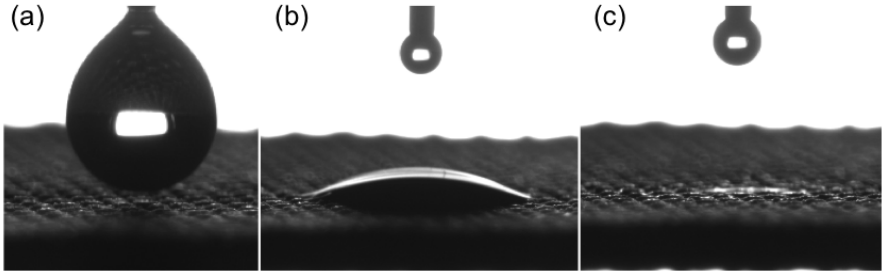

Fig. 8. Photographic images showing the absorption of a 4.0 μL water droplet into the uncoated 60 g/m^2 polyester Montana fabric (a - c). Image (a) corresponds to the droplet before contact with the fabric (0 ms), whilst images (b) and (c) show the droplet on the fabric after 80 and 160 ms respectively. The width of the needle is approximately 0.514 mm.

Superhydrophilicity commonly refers to the phenomenon of excess hydrophilicity, or attraction to water; in superhydrophilic materials, the contact angle of water is close 0°. Because it is difficult to measure the contact angle of a water droplet on a non-flat, inhomogeneous, surface, such as a fabric, herein a superhydrophilic surface is defined as the time taken for a water droplet is placed on the surface to lose its structure and be absorbed by the fabric. In the present work a superhydrophilic surface is defines as one where the water droplet merges with the substrate in a time less than 1 second.

3.2. Dip coating

Samples of each fabric were dip coated in a 20 wt.% aqueous solution of Al_{NP}-CAMO following the methodology previously reported [27]. The coated fabrics were characterized by contact angle measurements, SEM and associated EDX. During dip coating, the particles deposit onto the fabric and interact with the fabric's fibre's through physisorption. The mass uptake for each fabric was determined by measuring the mass before and after coating (e.g., Fig. 9). No coating was observed on the polyethylene because the fabric would not wet the aqueous solutions. The non-woven spunlace polypropylene fabrics show a significantly higher uptake in comparison with the woven fabrics. This is counter to the starting hydrophilicity, where the polyester and polyester/spandex blends would be expected to absorb the solution. Thus, suggesting that the starting wettability does not affect the CAMO loading. he uptake on the 55 g/cm^2 weight spunlace polypropylene is slightly greater than the 30 g/cm^2 materials, which would be expected based upon mass fiber per unit area.

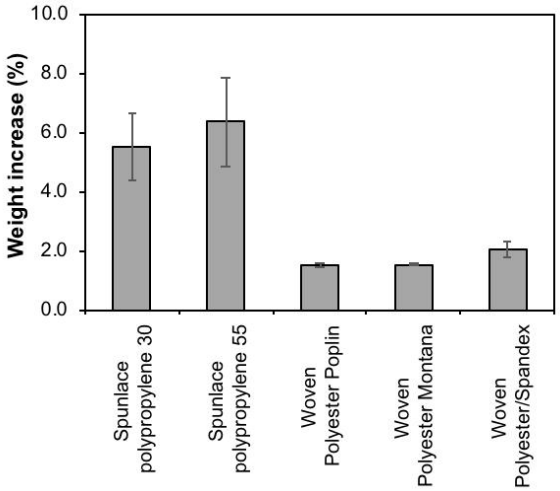

Fig. 9. Plot of mass uptake (%) for different woven and non-woven fabrics dip coated with a 20 wt.% aqueous solution of Al_{NP}-CAMO.

The large weight increase for the spunlace polypropylene fabrics when using 20 wt.% solution is accompanied by sloughing-off material during handling and webbing (as seen in the SEM, see Supplementary Materials) suggesting that a lower concentration solution is required. As a result, additional dip coat experiments to compare Al_{NP}-CAMO and Al_B-CAMO were performed using 1, 2, and 5 wt.% solutions. The uptake of Al_{NP}-CAMO and Al_B-CAMO on 55 g/cm^2 weight spunlace polypropylene was determined by measurement of the relative aluminum content by EDX using 1, 2, and 5 wt.% solutions under identical dip coat and drying conditions.

As may be seen from Fig. 10, the aluminum content (i.e., CAMO uptake) increases with the use of a 2 wt.% solution as compared 1 wt.% for both Al_{NP}-CAMO and Al_B-CAMO; however, further increase in solution concentration does not result in increased uptake. Presumably this signifies saturation of the fabric and further increases would necessitate multiple dip/dry cycles. Interestingly, Al_{NP}-CAMO shows a higher uptake that Al_B-CAMO at 1 wt.%, but this is reversed for higher concentrations.

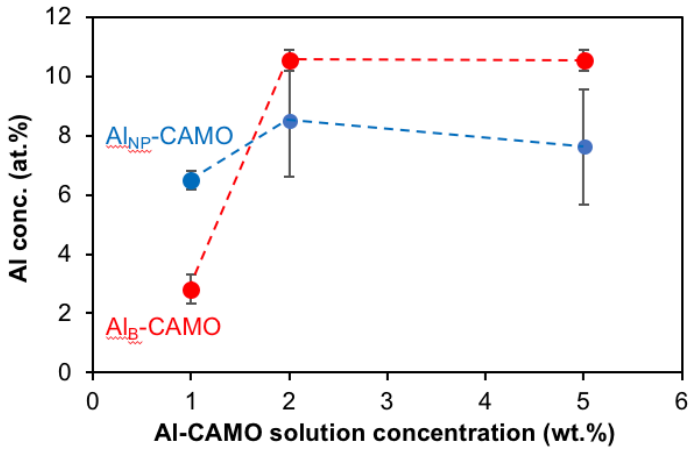

Fig. 10. Plot of aluminum concentration (at.%) as determined by EDX for 55 g/cm^2 weight spunlace polypropylene dip coated with aqueous solutions of Al$_{NP}$-CAMO and Al$_{B}$-CAMO.

3.3. Spray coating

Table 7 provides the data for spray coating of the fabrics by Al-CAMO or Fe-CAMO, which may be compared to the base fabrics in Table 6. Similarly to dip coating, during the spray coating the particles are deposited onto the fabric and interact with the fabric fibre through physisorption. In general, the performance of Al$_{B}$-CAMO and Al$_{NP}$-CAMO are either lower or comparable. In the case of polypropylene, the hydrophilicity is dramatically increased as indicated by the change from a contact angle for the untreated fabric of ca. 147° to <1 sec time for the droplet to collapse. Application of the functionalized nanoparticles onto the fabrics was observed to lower their wettability in most cases. For example, the initially hydrophilic polyester fabric becomes superhydrophilic after coating, while the Spandex changes from hydrophobic to superhydrophilic. In each case SEM images and associated EDX confirm the presence of a coating on the fabrics. Interestingly, the Montana polyester becomes less hydrophilic upon coating with either Al-CAMO or Fe-CAMO. A possible explanation for this could be that the coating material could slow the ingress of water into the fabric as the droplet is being adsorbed. The SEM images of uncoated and coated fabric (Fig. 11) shows that while the Al$_{NP}$-CAMO appears to have been deposited on the individual fibers, the coating is non-uniform and not contiguous. Given the application of spunlace polypropylene in PPE, and the significant enhanced hydrophilicity, further studies concentrated on this substrate.

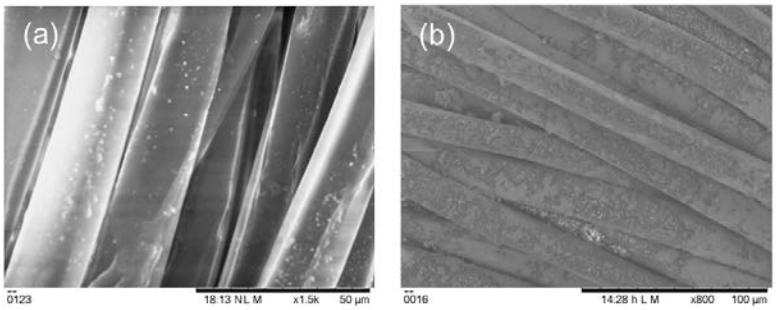

Fig. 11. SEM images of 60 g/cm^2 weight woven Montana polyester (a) before and (b) after spray coated with aqueous solutions of 5 wt.% Al_{NP}-CAMO.

Table 7

Summary of a spray coat conditions for the synthesis of M-CAMO (M = Al, Fe).

Fabric	Fabric weight (g/m^2)	Nanoparticles	Solution conc. (wt.%)	Number of 1 s coat steps	Water contact angle (°)[b]	Water absorption time (ms)[c]
Spunlace polypropylene	55	Al_{NP}-CAMO	1	3	n/a	102
Spunlace polypropylene	55	Al_{NP}-CAMO	2	3	n/a	96
Spunlace polypropylene	55	Al_{NP}-CAMO	5	3	n/a	103
Spunlace polypropylene	55	Al_{NP}-CAMO	1	3	88.2	n/a
Spunlace polypropylene	55	Al_{NP}-CAMO	5	1	n/a	160
Spunlace polypropylene	55	Al_{NP}-CAMO	1	5 mL [a]	86.6	n/a
Spunlace polypropylene	55	Al_{NP}-CAMO	1	10 mL [a]	56.8	n/a
Spunlace polypropylene	55	Al_{NP}-CAMO	1	15 mL [a]	n/a	15
Woven polyester/spandex	120	Al_{NP}-CAMO	1	1	n/a	4540
Woven polyester Poplin	62	Al_{NP}-CAMO	1	3	n/a	60
Woven polyester Montana	60	Al_{NP}-CAMO	1	3	n/a	2060
Spunlace polypropylene	55	Al_B-CAMO	1	3	110	n/a
Woven polyester Poplin	62	Al_B-CAMO	5	3	n/a	61
Woven polyester Montana	60	Al_B-CAMO	5	3	n/a	2060
Spunlace polypropylene	55	Fe-CAMO	1	3	n/a	1264
Spunlace polypropylene	55	Fe-CAMO	2	3	n/a	601
Spunlace polypropylene	55	Fe-CAMO	5	3	n/a	38
Spunlace polypropylene	55	FeO_x [b]	1	3	n/a	3820
Spunlace polypropylene	55	FeO_x [b]	2	3	n/a	3014
Spunlace polypropylene	55	FeO_x [b]	5	3	n/a	2620
Woven polyester/spandex	120	Fe-CAMO	5	1	26-61	n/a
Woven polyester Poplin	62	Fe-CAMO	5	1	n/a	320
Woven polyester Poplin	62	Fe-CAMO	5	3	n/a	80
Woven polyester Montana	60	Fe-CAMO	5	1	n/a	9660
Woven polyester Montana	60	Fe-CAMO	5	3	n/a	5000

[a] Total volume used. [b] Product from the reaction of $FeCl_2$ with NaOH without the addition of cysteic acid.

[b] The abbreviation "n/a" is used to show that water droplets did not remain on the top of the fabrics and as a result the contact angles could not be measured. Instead, the droplets were absorbed into the fabric in the times stated in column seven.

[c] The abbreviation n/a" is used to show that water droplets were not absorbed into the fabrics. Instead, they remained on the surface and showed the contact angles listed in column six.

As may be seen from Table 6 Al_{NP}-CAMO shows better results (in terms of reduced contact angle/increased hydrophilicity) than Al_B-CAMO for non-woven spunlace polypropylene, but near identical for Poplin; however, given the identical results obtained for films deposited on glass substrates (see above) this would suggest that the difference is due to the uptake on the fabric. Fig. 12 shows SEM images of spunlace polypropylene after spray coating with Al_B-CAMO (Fig. 12a and b) and Al_{NP}-CAMO (Fig. 12c and d). Fabric coated with Al_B-CAMO shows webbing even with a 1 wt.% solution and large deposits between the fibers using a 5 wt.% solution (c.f., Fig. 12a versus Fig. 12b). In contrast, spray coating with a 1 wt.% solution of Al_{NP}-CAMO shows no webbing (Fig. 12c), and even at 5 wt.% the webbing is contained (Fig. 12d). The uniformity of the spray coating may be seen from Fig. 13 showing the SEM image and associated EDX analysis of 55 g/cm^2 weight spunlace polypropylene dip coated with aqueous solutions of 2 wt.% Al_{NP}-CAMO.

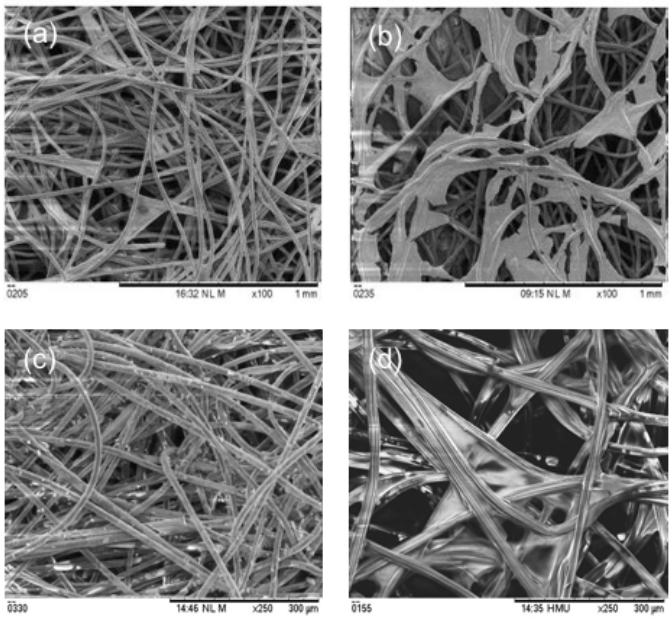

Fig. 12. SEM images of 55 g/cm^2 weight spunlace polypropylene dip coated with aqueous solutions of (a) 1 wt.% Al_B-CAMO, (b) 5 wt.% Al_B-CAMO, (c) 1 wt.% Al_{NP}-CAMO and (d) 5 wt.% Al_{NP}-CAMO.

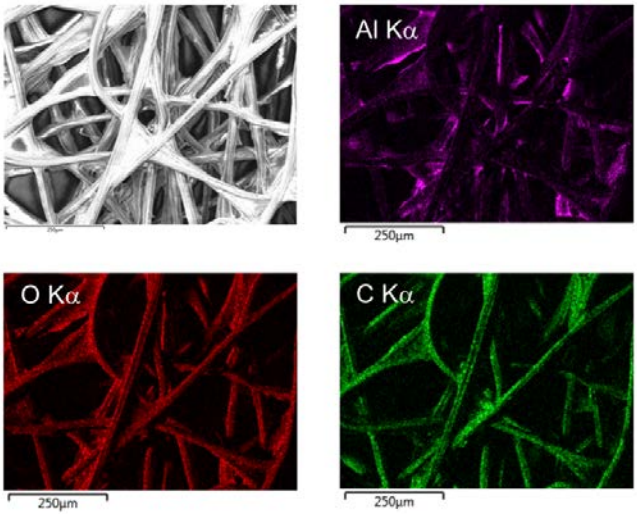

Fig. 13. SEM images and associated EDX maps of selected elements acquired at 15 kV using 10 minutes of acquisition time for a piece of the 55 g/m^2 non-woven polypropylene spunlace fabric after spray coating with 1 wt.% aqueous solution of Al_{NP}-CAMO showing the uniform distribution on the fabric fibers.

As an alternative to altering the solution concentration, a series of samples were prepared using a 1 wt.% solution of Al_{NP}-CAMO, but changing the total volume of solution sprayed. Increasing the solution volume results in a linear decrease in the contact angle for a water droplet on the fabric surface (Fig. 14). Importantly, at 15 mL of solution, the contact angle is not measured, but instead it collapses in 3780 ms suggesting that the fabric has reached superhydrophilicity.

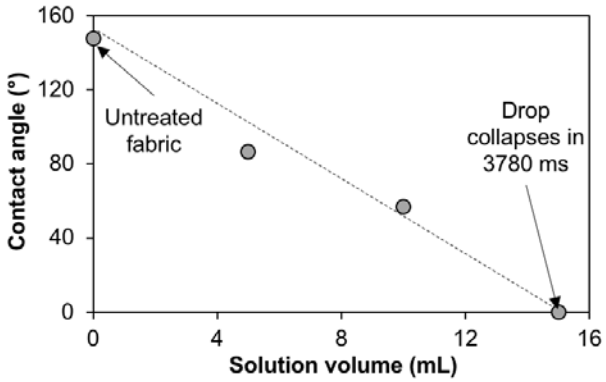

Fig. 14. Plots of contact angle (°) as a function of the volume of Al_{NP}-CAMO aqueous solution (1 wt.%) spray coated on 55 g/m^2 spunlace polypropylene fabric.

As may be seen from Table 6 the Fe-CAMO shows less of an effect in terms of contact angle reduction when compared to Al-CAMO. This is similar to the effects observed for superhydrophobic homologs [29] This is exemplified by Fig. 15, which shows a plot time for a water droplet to collapse (in ms) as a function of the mass increase after coating with 1, 2, and 5 wt.% solutions (using 3 × 1 sec coats). The AlNP-CAMO samples show essentially no change with increased mass of the coating, while the Fe-CAMO shows a more expected exponential decrease in time with mass added, i.e., the more Fe-CAMO added the more hydrophilic the surface. Thus, a 4% mass addition of Al_{NP}-CAMO has the same superhydrophilic performance of ca. 15-20% mass of Fe-CAMO. This is in agreement with the relative hydrophilicity of the materials (see above).

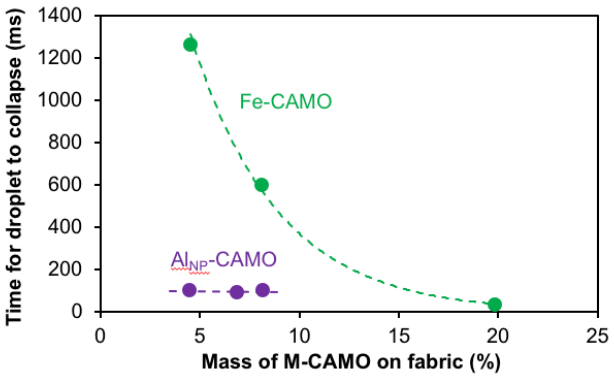

Fig. 15. Plots of time for a water droplet to collapse (ms) as a function of the percentage mass added on to 55 g/m^2 spunlace polypropylene fabric from a sprayed aqueous solution of (1, 2 and 5 wt.%) M-CAMO.

In order to be able to ascertain the effect of the cysteic acid as compared to the NP structure, samples of Fe-NPs were prepared by an analogous manner to Fe-CAMO, but without the addition of cysteic acid. As may be seen from Fig. 16 and Table 6, coating the spunlace polypropylene fabric with unfunctionalized Fe-NPs does increase the hydrophilicity of the fabric, but the cysteic acid functionality results in between 3× and 10× decrease in the time for a water droplet to collapse on the surface. This confirms our prior study of the cysteic acid's functionality being a controlling factor in creating a hydrophilic surface [21,22].

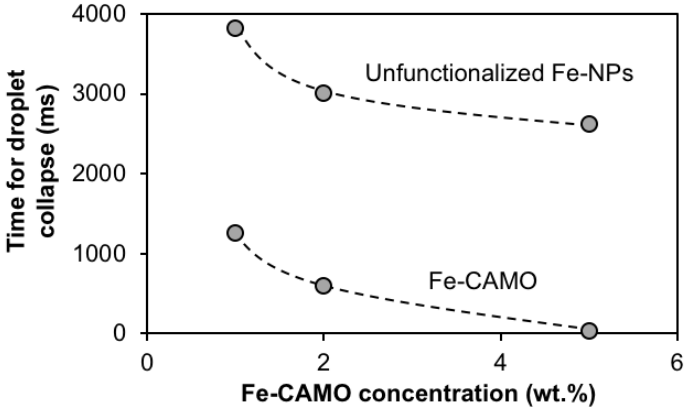

Fig. 16. Plots of time it takes for droplet to collapse (ms) as a function of the concentration of aqueous solution (wt.%) of Fe-CAMO and unfunctionalized Fe-NPs, spray coated on 55 g/m^2 spunlace polypropylene fabric.

4. Conclusions

Herein we report that a range of woven and non-woven fabrics may be dip and spray coated with aqueous solutions of cysteic acid functionalized metal oxide (CAMO) nanoparticles in order to increase their hydrophilic properties. The best performance for creating a superhydrophilic fabric is achieved by the use of Al-CAMO rather than Fe-CAMO. Furthermore, an excess of Al-CAMO does not greatly improve the performance meaning that ca. 5% mass uptake provides optimum superhydrophilic performance with no webbing and no sloughing. Finally, it appears that multiple passes of a sprayed solution create a more hydrophilic surface than a single pass for longer.

Acknowledgments

Financial support was provided by the Welsh Government Sêr Cymru 3 Program, the Reducing Industrial Carbon Emissions (RICE) operations funded by the Welsh European Funding Office (WEFO) through the Welsh Government, and SALTS Healthcare, Ltd. The authors declare no competing financial interest.

Appendix A. Supplementary materials.

Supplementary data associated with this article can be found, in the online version, at DOI: XXXXXX. SEM and associated EDX images; FT-IR spectra; photographs of fabrics and water droplets on fabric surfaces.

References

[1] G. R. Teesing, B. van Straten, P. de Man, T. Horeman-Franse, Is there an adequate alternative to commercially manufactured face masks? A comparison of various materials and forms. J. Hosp. Infect. 106 (2020) 246-253.

[2] J. E. Farnsworth, S. M. Goyal, S. W. Kim, T. H. Kuehn, P. C. Raynor, M. A. Ramakrishnan, S. Anatharaman, W. Tang, Development of a method for bacteria and virus recovery from heating, ventilation, and air conditioning (HVAC) filters. J. Environ. Monit. 8 (2006) 1006-1013.

[3] E. L. Anderson, P. Turnham, J. R. Griffin, C. C. Clarke, Consideration of the aerosol transmission for COVID-19 and public health. Risk Anal. 40 (2020) 902-907.

[4] J. Lelieveld, F. Helleis, S. Borrmann, Y. Cheng, F. Drewnick, G. Haug, T. Klimach, J. Sciare, H. Su, U. Pöschl, Model calculations of aerosol transmission and infection risk of COVID-19 in indoor environments. Int. J. Environ. Res. Public Health 17 (2020) 8114.

[5] G. P. Georgiou, A. Kilani, The use of aspirated consonants during speech may increase the transmission of COVID-19. Med. Hypotheses 144 (2020) 109937.

[6] B. Yao, Y. Wang, X. Ye, F. Zhang, Y. Peng, Impact of structural features on dynamic breathing resistance of healthcare face mask, Sci. Total Environ. 689 (2019) 743-753.

[7] E. Teirumnieks, I. Balchev, R. S. Ghalot, L. Lazov, Antibacterial and anti-viral effects of silver nanoparticles in medicine against COVID-19 - a review. Laser Phys. 31 (2021) 013001.

[8] G. Behbudi, Effect of silver nanoparticles disinfectant on covid-19. J. Adv. Appl. NanoBio Tech. 2 (2021) 63-67.

[9] N. Hutasoit, B. Kennedy, S. Hamilton, A. Luttick, R. A. R. Rashid, S. Palanisamy, Sars-CoV-2 (COVID-19) inactivation capability of copper-coated touch surface fabricated by cold-spray technology. Manuf. Lett. 25 (2020) 93-97.

[10] A. R. Barron, I. Powner, W. Al-Shatty, D. Hill, S. Kiani, A. Stanulis, L. Tretheway, S. Alexander, S. Winston, Coated substrate and articles with anti-viral properties, and fabrication processes, US Patent Application 17/336,169, June 2021.

[11] D. Chen, L. Tan, H. Liu, J. Hu, Y. Li, F. Tang, Fabricating superhydrophilic wool fabrics. Langmuir 26 (2010) 4675–4679.

[12] S. Houshyar, R. Padhye, R. A. Shanks, R. Nayak, Nanodiamond fabrication of superhydrophilic wool fabrics. Langmuir 35 (2019) 7105–7111.

[13] M. Ashraf, C. Campagne, A. Perwuelz, P. Champagne, A. Leriche, C. Courtois, Development of superhydrophilic and superhydrophobic polyester fabric by growing zinc oxide nanorods. J. Colloid Inter. Sci. 394 (2013) 545-553.

[14] L. Lao, L. Fu, G. Qi, E. P. Giannelis, J. Fan, Superhydrophilic wrinkle-free cotton fabrics via plasma and nanofluid treatment. ACS Appl. Mater. Interfaces 43 (2017) 38109–38116.

[15] J. Fang, A. Kelarakis, L. Estevez, Y. Wang, R. Rodriguez, E. P. Giannelis, Superhydrophilic and solvent resistant coatings on polypropylene fabrics by a simple deposition process. J. Mater. Chem. 20 (2010) 1651-1653.

[16] H. Chi, Z. Xu, Y. Ma, T. Tang, T. Zhang, Y. ZhaoMultifunctional highly oleophobic and superhydrophilic fabric coatings prepared by facile photopolymerization. Adv. Sustain. Syst. 4 (2020) 2000049.

[17] K. A. DeFriend, M. R. Wiesner, A. R. Barron, Alumina and aluminate ultrafiltration membranes derived from alumina nanoparticles. J. Membrane Sci. 224 (2003) 11-28.

[18] C. E. Bethley, C. L. Aitken, Y. Koide, C. J. Harlan, S. G. Bott, A. R. Barron, Structural characterization of dialkylaluminum carboxylates: models for carboxylate alumoxanes. Organometallics 16 (1997) 329-341.

[19] Y. Koide and A. R. Barron, $[Al_5(^tBu)_5(\mu_3\text{-}O)_2(\mu_3\text{-}OH)_3(\mu\text{-}OH)_2(\mu\text{-}O_2CPh)_2]$: A model for the interaction of carboxylic acids with boehmite. Organometallics 14 (1995) 4026-4029.

[20] S. Alexander, J. Eastoe, A. M. Lord, F. Guittard, A. R. Barron, Branched hydrocarbon low surface energy materials (LSEMs) for superhydrophobic nanoparticle derived surfaces. ACS Appl. Mater. Interfaces 8 (2016) 660-666.

[21] S. J. Maguire-Boyle, J. E. Huszman, T. J. Ainscough D. Oatley-Radcliffe, A. A. Alabdulkarem, S. F. Al-Mojil, and Andrew R. Barron, Superhydrophilic functionalization of micro-filtration ceramic membranes enables separation of hydrocarbons from frac and produced waters without fouling. Sci. Reports 7 (2017) 12267.

[22] S. J. Maguire-Boyle and A. R. Barron, A new functionalization strategy for oil/water separation membranes, J. Membrane Sci. 382 (2011) 107-115.

[23] W. Al-Shatty, A. M. Lord, S. Alexander, and A. R. Barron, Tunable surface properties of aluminum oxide nanoparticle from highly hydrophobic to highly hydrophilic. ACS Omega 2 (2017) 2507-2514.

[24] C. C. Landry, N. Pappè, M. R. Mason, A. W. Apblett, A. N. Tyler, A. N. MacInnes, and A. R. Barron, From minerals to materials: synthesis of alumoxanes from the reaction of boehmite with carboxylic acids. J. Mater. Chem. 5 (1995) 331-341.

[25] R. L. Callender, C. J. Harlan, N. M. Shapiro, C. D. Jones, D. L. Callahan, M. R. Wiesner, R. Cook, and A. R. Barron, Aqueous synthesis of water soluble alumoxanes: environmentally benign precursors to alumina and aluminum-based ceramics, Chem. Mater. 9 (1997) 2418-2433.

[26] R. L. Callender and A. R. Barron, A novel route to alumina and aluminate coatings on SiC, carbon and Kevlar® fiber-reinforced ceramic matrix composites using carboxylate-alumoxane nanoparticles. J. Mater. Res. 15 (2000) 2228-2237.

[27] S. J. Maguire-Boyle, M. V. Liga, Q. Li, and A. R. Barron, Alumoxane/ferroxane nanoparticles for the removal of viral pathogens: the importance of surface functionality to nanoparticle activity. Nanoscale 4 (2012) 5627-5632.

[28] J. Rose, M. M. Cortalezzi-Fidalgo, S. Moustier, C. Magnetto, C. D. Jones, A. R. Barron, M. R. Wiesner, and J.-Y. Bottero, Synthesis and characterization of carboxylate-FeOOH nanoparticles (ferroxanes) and ferroxane-derived ceramics, Chem. Mater. 14 (2002) 621-628.

[29] D. Hill, A. R. Barron, and S. Alexander, Comparison of hydrophobicity and durability of functionalized aluminium oxide nanoparticle coatings with magnetite nanoparticles–links between morphology and wettability. J. Colloid Interface Sci. 555 (2019) 323-330.

[30] Y. V. Kolen'ko, M. Bañobre-López, C. Rodríguez-Abreu, E. Carbó-Argibay, A. Sailsman, Y. Piñeiro-Redondo, M. F. Cerqueira, D. Y. Petrovykh, K. Kovnir, O. I. Lebedev, J. Rivas, Large-scale synthesis of colloidal fe3o4 nanoparticles exhibiting high heating efficiency in magnetic hyperthermia. J. Phys. Chem. C 118 (2014) 8691–8701.

[31] Y. Lee, J. Lee, C. J. Bae, J.-G. Park, H.-J. Noh, J.-H., Park, T. Hyeon, Large-scale synthesis of uniform and crystalline magnetite nanoparticles using reverse micelles as nanoreactors under reflux conditions. Adv. Funct. Mater. 15 (2005) 503-509.

[32] L. Morrow and A. R. Barron, Issues affecting the synthetic scalability of ternary metal ferrite nanoparticles. J. Nanoparticles 2015 (2015) 105862.

[33] C. T. Vogelson and A. R. Barron, Particle size control and dependence on solution pH of carboxylate-alumoxane nanoparticles. J. Non-Cryst. Solids 290 (2001) 216-223.

[34] C.F. Whitehead, R.F. Carbonaro, A.T. Stone, Adsorption of benzoic acid and related carboxylic acids onto FeOOH (Goethite): the low ionic strength regime. Aquat. Geochem. 21 (2015) 99-121.

[35] H. Cui, Y. Liu, W. Ren, Structure switch between α-Fe_2O_3, γ-Fe_2O_3 and Fe_3O_4 during the large scale and low temperature sol–gel synthesis of nearly monodispersed iron oxide nanoparticles. Adv. Powder Technol. 24 (2013) 93-97.

Graphical Abstract

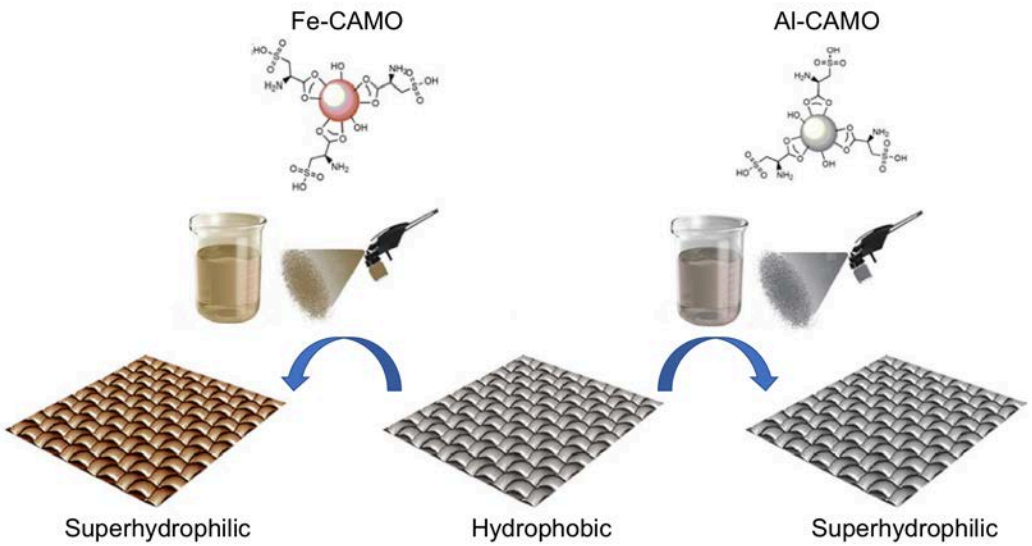
Fe-CAMO
Al-CAMO
Superhydrophilic
Hydrophobic
Superhydrophilic